J. Fluid Mech. (1999), *vol.* 387, *pp.* 205–226. Printed in the United Kingdom

Three-dimensional destabilization of Stuart vortices: the influence of rotation and ellipticity

By P. G. POTYLITSIN AND W. R. PELTIER

Department of Physics, University of Toronto, Toronto, Ontario, Canada M5S 1A7

(Received 2 February 1998 and in revised form 7 December 1998)

We investigate the influence of the ellipticity of a columnar vortex in a rotating environment on its linear stability to three-dimensional perturbations. As a model of the basic-state vorticity distribution, we employ the Stuart steady-state solution of the Euler equations. In the presence of background rotation, an anticyclonic vortex column is shown to be strongly destabilized to three-dimensional perturbations when background rotation is weak, while rapid rotation strongly stabilizes both anticyclonic and cyclonic columns, as might be expected on the basis of the Taylor–Proudman theorem. We demonstrate that there exist three distinct forms of three-dimensional instability to which strong anticyclonic vortices are subject. One form consists of a Coriolis force modified form of the 'elliptical' instability, which is dominant for vortex columns whose cross-sections are strongly elliptical. This mode was recently discussed by Potylitsin & Peltier (1998) and Leblanc & Cambon (1998). The second form of instability may be understood to constitute a three-dimensional inertial (centrifugal) mode, which becomes the dominant mechanism of instability as the ellipticity of the vortex column decreases. Also evident in the Stuart model of the vorticity distribution is a third 'hyperbolic' mode of instability that is focused on the stagnation point that exists between adjacent vortex cores. Although this short-wavelength cross-stream mode is much less important in the spectrum of the Stuart model than it is in the case of a true homogeneous mixing layer, it nevertheless does exist even though its presence has remained undetected in most previous analyses of the stability of the Stuart solution.

1. Introduction

Large-scale vortices play an important role in the dynamics of the atmosphere and ocean. Such quasi-two-dimensional structures are clearly visible in satellite images, which can provide essential information concerning vortex formation, characteristic spatial scale and lifetime. It is often found to be the case that individual vortices with vertically oriented axes may be organized so as to form extended coherent structures such as vortex streets. Examples of such structures are described, for example, in Etling (1990) and Potylitsin & Peltier (1998) who discuss the von Kármán vortex streets that are often observed to develop in the lee of Jan Mayen island in the Norwegian Sea. The development of such two-dimensional trains of vortices, in which individual vortex axes are oriented vertically, may often occur through the barotropic instability mechanism of quasi-two-dimensional flows, which have embedded large-scale shear in horizontal velocity.

One of the most important and interesting questions concerning the dynamics of such two-dimensional coherent structures is their stability to three-dimensional fluctuations. It is clear that the two-dimensional evolution of such vorticity distributions will not depend on the background rotation if the influence of rotation is considered from the f-plane perspective and if the axis of rotation is parallel to the axis of the vortices in the developed two-dimensional flow. In such circumstances two-dimensional evolution of the flow may be studied through numerical solution of the two-dimensional nonlinear (barotropic) dynamical system which includes the influence of neither stratification nor background rotation.

Only in very special circumstances, however, will such flows remain two-dimensional. Close examination of both satellite images of atmospheric flows and related laboratory experiments reveals that anticyclonic vortex columns tend to be more unstable than cyclonic columns. This may on occasion lead to the development of a broken symmetry in the vorticity distribution in a vortex street such that anticyclonic vortices do not appear. This broken symmetry is clearly evident in the satellite photos described in Etling (1990) (see figure 5 in particular) and Potylitsin & Peltier (1998) (see figure 1*b*).

Laboratory experiments that have been specifically designed to investigate the evolution of mixing layers (e.g. Wygnanski *et al.* 1979; Browand & Ho 1983) have demonstrated that fully three-dimensional motions invariably arise even though the flow may tend to remain quasi-two-dimensional on the scale of the large vortices. Hopfinger, Browand & Gagne (1982) have also observed the presence of intense cyclonic vortices and much weaker anticyclones in the field of turbulence produced with an oscillating grid in a deep rotating tank. In the rotating environment the turbulence produced by the oscillation of the grid also leads to the formation of long-lived vortices, which do not appear in the non-rotating case. Experimental analyses of the evolution of barotropic vortices in a rotating environment by Kloosterziel & van Heijst (1991) have also demonstrated that the behaviour of initially two-dimensional cyclonic and anticyclonic vortices differs dramatically at moderate Rossby numbers. In this experimental work it has been observed that a barotropic cyclonic vortex is gradually transformed into a stable tripolar structure consisting of a cyclonic core and two weaker anticyclonic satellites. On the other hand, an anticyclonic vortex tends to be more unstable and in fact exhibits 'explosively' unstable behaviour, which leads inevitably to an immediate split of the vortex column into two dipolar structures.

Theoretical analyses of the stability of non-rotating vortex columns have revealed that such two-dimensional vorticity distributions do indeed support three-dimensional linear secondary instabilities. The ellipticity of the streamlines in the vortex cores of the basic-state flow, in particular, has been shown to be responsible for the existence of a so-called translative or elliptical instability. Early analyses of the three-dimensional stability properties of the Stuart vortex train by Pierrehumbert & Widnall (1982), Pierrehumbert (1986) and Bayly (1986) were the first to reveal the existence of this elliptical instability, which has the property that no short-wave cutoff exists in the absence of dissipation. The streamwise wavelength of this instability equals that of the basic flow while the cross-stream wavelength is only marginally shorter and the structure of the instability is such as to lead to the periodic bending of the vortex columns. In the work by Waleffe (1990) a physical interpretation of the breakdown of two-dimensional elliptical flows via this mechanism has been proposed. The results of these analyses are suggestive of a universal mechanism through which complex three-dimensional motion might develop on two-dimensional elliptical vortex columns.

In a sequence of detailed analyses, Klaassen & Peltier (1985*b*, 1989, 1991) investi-

gated the stability of a two-dimensional train of finite-amplitude Kelvin–Helmholtz waves to arbitrary three-dimensional perturbations. They focused upon the role of transverse secondary instability on the evolution of such Kelvin–Helmholtz billows, a basic state which differs significantly from the Stuart model that had been chosen as the basis for analysis by Pierrehumbert & Widnall (1982). The analysis of such vortex trains also revealed the existence of a braid-centred mode of instability, which had not been found in the original work on the spectrum of the Stuart model and which derives from what we might refer to as 'hyperbolic' instability. Higher resolution analyses of the Stuart vortex by Klaassen & Peltier (1991), however, also confirmed the existence of this mode although with a lower growth rate than that which was obtained for the Kelvin–Helmholtz model. The hyperbolic stagnation points between adjacent vortex cores of the basic state train of Kelvin–Helmholtz waves are the regions within which this instability concentrates. The authors suggested that this 'hyperbolic' instability is the mechanism which is responsible for the streamwise vortex streaks whose appearance is precursory to the turbulent collapse of the unstratified mixing layer rather than the elliptical mode.

Numerical analyses of the evolution of the braid region between adjacent vortices were also performed by Corcos & Lin (1984), although their work was not formulated in terms of the search for a secondary linear instability of the highly nonlinear two-dimensional basic-state flow; rather they sought to explain the appearance of streamwise vortex streaks in terms of a non-linear 'collapse' process. The linear secondary 'hyperbolic' mode of instability was however fully confirmed in the more refined theoretical analyses of the three-dimensional stability of two-dimensional Kelvin–Helmholtz billows by Smyth & Peltier (1991, 1994). Full three-dimensional nonlinear simulations of shear flow evolution have also been performed by Caulfield & Peltier (1994) to further confirm that the new 'hyperbolic instability' actually dominates in an unconstrained three-dimensional flow which is evolving in time so long as the stratification is sufficiently weak. In such simulations the characteristic streamwise streaks of vorticity between adjacent vortex cores develop spontaneously. It was of course on the basis of earlier laboratory experiments that it was first revealed that it was in the braid regions between adjacent vortex cores rather than in the elliptical cores themselves that intensive three-dimensional motions originated. The 'rib' vortices that are now known to develop as a consequence of hyperbolic instability were observed in the braid regions between adjacent vortices in unstable plane mixing layers by Bernal & Roshko (1986), Lasheras, Cho & Maxworthy (1986), Lasheras & Choi (1988), Nygaard & Glezer (1991) and Schowalter, Van Atta & Lasheras (1994).

Further investigations of the three-dimensional stability of columnar vortices in the presence of rotation have recently been discussed by Smyth & Peltier (1994). These authors focused their attention upon the question of the linear stability of a train of Kelvin–Helmholtz vortices with vertically oriented axes on the so-called f-plane. The existence of both elliptical and hyperbolic modes of instability was confirmed in these analyses, which also revealed the existence of a new 'edge mode' of three-dimensional instability. This instability was found to inhabit the region surrounding anticyclonic vortex cores at moderate Rossby numbers. In the subsequent work by Potylitsin & Peltier (1998) these analyses were extended to incorporate density stratification parallel to the axes of both Kelvin–Helmholtz and 'Kida-like' vortices (e.g. see Kida 1981; Potylitsin & Peltier 1998). In this work an additional mode of elliptical instability modified by the Coriolis force was also discovered for anticyclonic vortices at moderate Rossby numbers.

Leblanc & Cambon (1998) have very recently analysed the linear stability of Stuart

vortices in the presence of the Coriolis force and also noted the destabilization of Stuart vortices by weak anticyclonic rotation. Building on the earlier work of Cambon *et al.* (1994) they also attempted to further clarify the physical mechanism of the instability using local linear instability theory. However, their analysis failed to identify the existence of either the 'edge' mode of Smyth & Peltier (1994) or the 'hyperbolic' mode of Klaassen & Peltier (1991) when this model of the basic state was employed. Their analyses have therefore called into question the results of both Klaassen & Peltier (1991) for the non-rotating Stuart model and Potylitsin & Peltier (1998) for the rotating Kelvin–Helmholtz model.

Carnevale *et al.* (1997) have recently focused upon a model system consisting of an isolated Gaussian columnar vortex and investigated the way in which the three-dimensional instability of the unstratified vortex column evolves at finite amplitude. These fully three-dimensional simulations also revealed extreme differences in the behaviour of cyclonic and anticyclonic vortices. The selective destruction of anticyclones at moderate Rossby number has also been very clearly revealed in the numerical simulation of rotating turbulence in homogeneous three-dimensional fluid by Bartello, Metais & Lesieur (1994), whose work in fact motivated the original theoretical analyses of Smyth & Peltier (1994).

The results obtained in these numerical simulations may be explained only by the presence of three-dimensional secondary circulation in the flow. The initial analyses of the linear stability of a barotropic vortex column on the f-plane, based upon the Kelvin–Helmholtz model, clearly demonstrated the existence of a three-dimensional instability to which anticyclonic vortex columns are selectively subject in circumstances in which the Rossby number is moderate (i.e. of order unity). This mechanism arises in flow with relatively weak background rotation which tends to reduce the absolute vorticity of an anticyclonic vortex to a value near zero and, thereby, to destabilize the flow. It will be noted on the basis of the above discussion that there do therefore exist three distinct forms of three-dimensional instabilities to which strong anticyclonic vortex columns are subject. One form may be identified as an elliptical instability modified by the Coriolis force. This type of instability has been clearly identified in the recent work by Potylitsin & Peltier (1998) and Leblanc & Cambon (1998). The second form may be understood to constitute a three-dimensional inertial (centrifugal) instability which appears on the edge of the anticyclonic columnar vortex (Smyth & Peltier 1994; Potylitsin & Peltier 1998). Also evident in these rotating flows is the same 'hyperbolic' instability that is focused on the stagnation point that exists between adjacent vortices in a vortex train that is not subject to rotation. It has already been shown that this mode of instability achieves its maximum growth rate in the vicinity of zero background rotation but continues to persist for non-zero values of background rotation.

Our goal in this paper is to provide a detailed assessment of the circumstances in which these unstable modes may appear as well as to make a connection between the three distinct types of three-dimensional instabilities that are supported by strong anticyclones. In particular we will investigate thoroughly the influence of the ellipticity of the vortex streamlines on the mechanism of three-dimentional instability. This influence was only briefly described in the previous analysis by Potylitsin & Peltier (1998) and our goal in the present paper is to provide a systematic investigation of this effect. One of the greatest concerns in the present context, however, is to address issues arising from the fact that Leblanc & Cambon (1998) found no evidence of the existence of either the 'edge' or 'hyperbolic' instabilities for the single highly elliptical vortex whose stability they analysed. Our primary goal in the present paper will therefore be to demonstrate that these modes do in fact also exist for the rotating Stuart model.

In the analyses of this issue that form the core of the present paper, we will therefore employ the Stuart model (Stuart 1967) with various values of the ellipticity parameter of the vorticity distribution. Stuart vortices are often considered to constitute a useful stationary inviscid model of a two-dimensional shear layer with embedded co-rotating columnar vortices. The advantage of this model is that the ellipticity of the vortices can be easily varied, which will allow us to investigate the influence of ellipticity on the mechanisms of three-dimensional instability. Our analyses will pertain to the regime of moderately high Rossby number, for a reason that will become apparent below. By comparing the results of analyses performed for different values of the ellipticity of the vortex column, we will reveal the circumstances in which one or another of the above discussed three mechanisms of instability becomes dominant.

In the next section of the paper we will review the theoretical methods that we have previously developed to enable detailed investigation of the broad class of problems in which the issue of the stability of two-dimensional flow to arbitrary three-dimensional perturbations arises. Section 3 is devoted to the presentation and analysis of the results that we have obtained by applying this theoretical formalism to analyse the stability of Stuart vortices as a function of their ellipticity. Conclusions are summarized in § 4.

2. Methodology

The formalism for multi-dimensional stability analysis that we will employ was originally developed by Klaassen & Peltier (1985*b*, 1989, 1991) and by Smyth & Peltier (1989, 1991, 1994), and has recently been extended so as to incorporate the influence of a stable density stratification parallel to the axis of a two-dimensional vortex by Potylitsin & Peltier (1998). In the present work our attention will be restricted to the investigation, in the case of inviscid unstratified flow, of the linear stability of a periodic row of columnar vortices arranged as in figure 1 and described by the Stuart model. The geophysically unconventional labelling of the coordinate axes has been employed so as to maintain consistency with previous analyses in which the coordinate direction normal to the mean flow was taken to be the z-direction. If the angular velocity Ω is taken to represent the Earth's rotation, then our x-, y- and z-axes would denote the zonal, vertically downward and meridional directions, respectively.

2.1. *The two-dimensional Stuart model of the vorticity distribution*

Stuart (1967) reported the existence of a family of steady solutions of the two-dimensional Euler equations, the non-dimensional stream function for which is given by the expression

$$\psi = -\frac{(1-\rho)^2}{1-\rho^2}\log[\cosh(z - H/2) + \rho\cos x] \tag{2.1}$$

while the corresponding non-dimensional vorticity has the form

$$\omega = \left(\frac{1-\rho}{\cosh(z - H/2) + \rho\cos x}\right)^2 \tag{2.2}$$

in which ρ is the ellipticity parameter, which lies in the range $0 \leqslant \rho < 1$. Note that (2.1) and (2.2) have been non-dimensionalized in terms of the length scale L which equals the total length of the domain (see figure 1) and the velocity scale U which equals

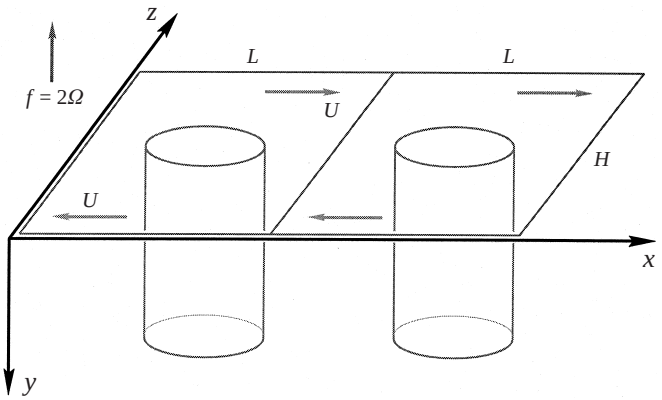

FIGURE 1. The definition of the coordinate system. The system rotates along the y-axis with the angular velocity $\Omega = f/2$, where f is the Coriolis parameter. L and H are the x- and z-dimensions of the computational domain. U is the velocity scale of the shear layer.

half the total change in velocity across the shear layer. The non-dimensionalization procedure is slightly different from that employed in previous studies by Smyth & Peltier (1994) and Potylitsin & Peltier (1998) where the fundamental length scale was taken to be h which equals half the total depth of the shear layer. Note also that the maximum value of the non-dimensional vorticity is equal to one for any value of the vortex parameter ρ.

The exact Stuart solution of the steady-state Euler equations given by (2.1) and (2.2) describes a shear layer centred on the line $z = H/2$ between two uniform streams. Indeed $U = \pm(1-\rho)^2/(1-\rho^2)$ and $W = 0$ as $z \to \pm\infty$. The value of $\rho = 0$ corresponds to the hyperbolic tangent parallel shear flow $U = (1-\rho)^2 \tanh(z - H/2)/(1-\rho^2)$, while in the limit $\rho \to 1$ the Stuart solution describes a single 2π-periodic row of co-rotating point vortices aligned along the x-axis.

The Stuart model has several limitations as a model of the nonlinear waves that are physically realizable in a shear flow. Both experimental (Winant & Browand 1974) and numerical (Corcos & Sherman 1984) studies of shear flows have demonstrated that the vorticity between two adjacent vortex cores is compressed into thin strands or filaments often referred to as 'braids', while the Stuart solution does not contain these structures. The most unstable mode of the hyperbolic tangent shear flow has non-dimensional streamwise wavenumber $\alpha = 0.44$, while the Stuart vortices (wavenumber $\alpha = 1$) have about half the wavelength of physically realized disturbances. Furthermore, unsteady behaviour (Klaassen & Peltier 1985*a*; Potylitsin & Peltier 1998) in the form of vortex nutation is clearly evident in the mixing layer and is not described by the Stuart model. However, the Stuart vortex may nevertheless provide a useful model of columnar vortices in shear flow, so long as we bear these limitations in mind.

In the present context we will employ the Stuart model with three different values of the vortex parameter ρ: namely 0.33, 0.50 and 0.75. As the vortex parameter ρ increases, the ellipticity of the Stuart vortex decreases (see figure 2), and the vortex transforms from the elliptical form (figure 2*a*), where the elliptical instability is expected to play a crucial role, to an almost circular form (figure 2*c*), where we might reasonably expect the centrifugal instability of Smyth & Peltier (1994) to dominate. Therefore stability analyses of the Stuart vortex for different values of the vortex parameter ρ will reveal the influence of the ellipticity of the vortex on its stability characteristics and will allow us to fully understand the nature of the connection

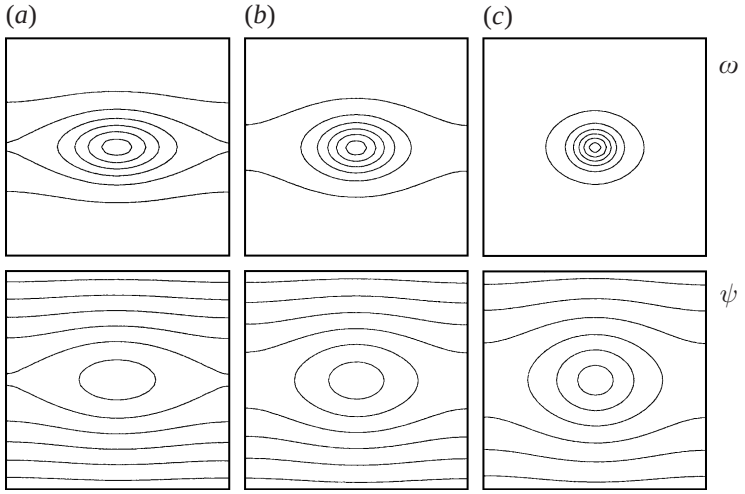

FIGURE 2. The two-dimensional vorticity ω and stream function ψ in the (X,Z)-plane for the Stuart vortices with various values of the vortex parameter ρ: (*a*) $\rho = 0.33$ (highly elliptical vortex), (*b*) $\rho = 0.50$ (moderately elliptical vortex), (*c*) $\rho = 0.75$ (vortex with low ellipticity).

between the results obtained by Potylitsin & Peltier (1998) for the Kelvin–Helmholtz model and by Leblanc & Cambon (1998) for the Stuart model with high ellipticity.

2.2. *Three-dimensional stability theory for two-dimensional coherent vortex structures in rotating flow*

In this section we will discuss the mathematical methods that have been developed to analyse the three-dimensional linear stability of the Stuart model of the vorticity distribution described in the last section. In the present context we will restrict our attention to the unstratified and inviscid case (the Froude number $Fr = U/(NL)$, in which N is the buoyancy frequency, will be assumed to be infinite), which simplifies the mathematical formalism substantially. In what follows, we will provide only a brief summary of the basic methodology and highlight a number of details not previously enumerated.

The momentum conservation and continuity equations for three-dimensional, incompressible and rotating flow in the f-plane approximation are

$$\boldsymbol{U}_t + (\boldsymbol{U}\cdot\nabla)\boldsymbol{U} = -\frac{1}{\rho}\nabla p - \boldsymbol{f}\times\boldsymbol{U}, \tag{2.3a}$$

$$\nabla\cdot\boldsymbol{U} = 0. \tag{2.3b}$$

The method of analysis that we will employ is based upon a linearization of the momentum balance equations. These are linearized in perturbations about a basic two-dimensional state which is independent of the spanwise (y) coordinate. Assuming, without loss of generality, that three-dimensional perturbations vary sinusoidally in the spanwise direction parallel to the axis of the vortex column, we may expand the three-dimensional fields Φ as

$$\Phi(x,y,z,t) = \tilde{\Phi}(x,z,t) + \hat{\phi}(x,z,t)\mathrm{e}^{\mathrm{i}dy}, \quad \hat{\phi}(x,z,t) \ll \tilde{\Phi}(x,z,t) \tag{2.4}$$

in which $\tilde{\Phi}$ is the corresponding field of the barotropic basic state, $\hat{\phi}$ represents the complex amplitude of the corresponding perturbation to the basic state and d denotes the spanwise wavenumber.

The linearized momentum balance and continuity equations that determine the evolution of small-amplitude perturbations can be written in the form of the following linear partial differential equations:

$$\hat{u}_t = -\tilde{U}\hat{u}_x - \tilde{U}_x\hat{u} - \tilde{W}\hat{u}_z - \tilde{U}_z\hat{w} - \hat{p}_x + \frac{1}{Ro}\hat{w}, \tag{2.5a}$$

$$\hat{v}_t = -\tilde{U}\hat{v}_x - \tilde{W}\hat{v}_z - \mathrm{i}d\hat{p}, \tag{2.5b}$$

$$\hat{w}_t = -\tilde{U}\hat{w}_x - \tilde{W}_x\hat{u} - \tilde{W}\hat{w}_z - \tilde{W}_z\hat{w} - \hat{p}_z - \frac{1}{Ro}\hat{u}, \tag{2.5c}$$

$$\hat{u}_x + \mathrm{i}d\hat{v} + \hat{w}_z = 0, \tag{2.5d}$$

in which the Rossby number $Ro = U/fL$ and the pressure scale is $[\hat{p}] = \rho_0 U^2$.

Combining partial derivatives with respect to the corresponding spatial variable of each of the x-, y- and z-coordinate momentum balance equations in (2.5) with the continuity equation (2.5d), a diagnostic equation for the pressure is obtained that has the following form:

$$\Delta\hat{p} = -\frac{1}{Ro}(\hat{u}_z - \hat{w}_z) - 2(\tilde{U}_x\hat{u}_x + \tilde{U}_z\hat{w}_x + \tilde{W}_x\hat{u}_z + \tilde{W}_z\hat{w}_z) \tag{2.6}$$

which now replaces the continuity equation (2.5d).

To solve the set of linear partial differential equations (2.5) together with the diagnostic equation for pressure (2.6) we restrict attention to the domain $0 \leqslant x \leqslant L$, $0 \leqslant z \leqslant H$. The boundary conditions on the amplitudes of the three-dimensional perturbations in the z-direction are, on $z = 0, H$,

$$\hat{u}_z = \hat{v}_z = \hat{w} = \hat{p}_z = 0. \tag{2.7}$$

The pressure and velocity perturbations are assumed to exhibit the same periodicity in the streamwise direction as does the basic-state two-dimensional flow so that sub-harmonic instability is suppressed. Therefore, the x- and z-dependence of the problem may be represented spectrally as a sum of orthogonal functions by applying the Galerkin formalism. Using this technique the velocity and pressure perturbations may be expanded as

$$\begin{pmatrix} \hat{u} \\ \hat{v} \\ \hat{p} \end{pmatrix} = \begin{pmatrix} u_{\lambda v} \\ v_{\lambda v} \\ p_{\lambda v} \end{pmatrix} F_{\lambda v}, \quad \hat{w} = w_{\lambda v} G_{\lambda v}, \tag{2.8}$$

in which it is understood that repeated indices are to be summed over. The complete set of orthogonal functions is defined as

$$F_{\lambda v} = \mathrm{e}^{\mathrm{i}\lambda\alpha x} \cos\frac{v\pi}{H} z, \tag{2.9a}$$

$$G_{\lambda v} = \mathrm{e}^{\mathrm{i}\lambda\alpha x} \sin\frac{v\pi}{H} z. \tag{2.9b}$$

The orthogonal functions $F_{\lambda v}$ and $G_{\lambda v}$ are selected so that the boundary conditions on $z = 0, H$ are satisfied automatically.

It is worth noting that if the solutions of interest had appreciable amplitude near the boundaries $z = 0, H$, then the boundary condition for $\hat{p}$ would need to be replaced by $\hat{p}_z = -Ro^{-1}\hat{u}$. It would therefore follow, in the case in which f is non-zero, that the pressure perturbation would be expanded in terms of the $G_{\lambda v}$ rather than $F_{\lambda v}$ to take into account the Coriolis force. Therefore, coefficients of the stability matrix

$A^{\kappa\mu}_{\lambda\nu}(t)$ (see below) would have slightly different forms. In the present application, the eigenfunctions of the stability problem are localized far from the rigid boundaries and there is no appreciable difference between the results obtained using the two different sets of boundary conditions on $z = 0, H$, namely $\hat{p}_z = 0$ or $\hat{p}_z = -Ro^{-1}\hat{u}$.

By substituting expansions (2.8) into (2.5) and (2.6) and computing the inner products $\langle F^*_{\kappa\mu}\bullet\rangle$ or $\langle G^*_{\kappa\mu}\bullet\rangle$ with each equation, where $\bullet$ represents any equation of the set (2.5) and (2.6) and in which the symbol $*$ denotes complex-conjugation, the final set of equations may be derived. The pressure may clearly be eliminated from the system (2.5) using the diagnostic equation (2.6). The inner product is explicitly

$$\langle\star\rangle = \frac{\alpha}{\pi H}\int_0^{2\pi/\alpha} \mathrm{d}x \int_0^H \star\, \mathrm{d}z. \tag{2.10}$$

Application of this procedure reduces the system of partial differential equations to a set of linear ordinary differential equations. In following this sequence of steps it is important to note that $\langle F^*_{\kappa\mu}F_{\lambda\nu}\rangle = \delta_{\lambda\nu}\delta_{\mu\nu}(1+\delta_{\mu 0})$ and $\langle G^*_{\kappa\mu}G_{\lambda\nu}\rangle = \delta_{\lambda\nu}\delta_{\mu\nu}(1-\delta_{\mu 0})$. These operations reduce (2.5) and (2.6) to the following matrix form:

$$\frac{\mathrm{d}}{\mathrm{d}t}\begin{pmatrix} u_{\kappa\mu} \\ v_{\kappa\mu} \\ w_{\kappa\mu} \end{pmatrix} = \begin{pmatrix} \langle UU\rangle^{\kappa\mu}_{\lambda\nu} & 0 & \langle UW\rangle^{\kappa\mu}_{\lambda\nu} \\ \langle VU\rangle^{\kappa\mu}_{\lambda\nu} & \langle VV\rangle^{\kappa\mu}_{\lambda\nu} & \langle VW\rangle^{\kappa\mu}_{\lambda\nu} \\ \langle WU\rangle^{\kappa\mu}_{\lambda\nu} & 0 & \langle WW\rangle^{\kappa\mu}_{\lambda\nu} \end{pmatrix} \begin{pmatrix} u_{\lambda\nu} \\ v_{\lambda\nu} \\ w_{\lambda\nu} \end{pmatrix}. \tag{2.11}$$

It is now obvious that the set of equations for $v_{\kappa\mu}$ decouples from the system and in order to reduce the dimension of the matrix one may remove these equations from (2.11) because $u_{\kappa\mu}$ and $w_{\kappa\mu}$ do not depend on $v_{\lambda\nu}$. Applying this reduction leads finally to the following set of ordinary differential equations:

$$\frac{\mathrm{d}}{\mathrm{d}t}\begin{pmatrix} u_{\kappa\mu} \\ w_{\kappa\mu} \end{pmatrix} = \begin{pmatrix} \langle UU\rangle^{\kappa\mu}_{\lambda\nu} & \langle UW\rangle^{\kappa\mu}_{\lambda\nu} \\ \langle WU\rangle^{\kappa\mu}_{\lambda\nu} & \langle WW\rangle^{\kappa\mu}_{\lambda\nu} \end{pmatrix} \begin{pmatrix} u_{\lambda\nu} \\ w_{\lambda\nu} \end{pmatrix} \tag{2.12}$$

and to a diagnostic equation for the velocity component $v_{\kappa\mu}$, namely

$$v_{\lambda\nu} = -\frac{\lambda\alpha}{d}u_{\lambda\nu} + \frac{\mathrm{i}D_\nu}{d}w_{\lambda\nu}, \tag{2.13}$$

in which $D_\nu = \nu\pi/H$. Note also that element $\omega_{\lambda\nu(\nu=0)}$ does not influence the velocity perturbation field because $G_{\lambda\nu(\nu=0)} \equiv 0$. Therefore the corresponding matrix elements can also be removed from equation (2.12).

Owing to the finite memory of available computers, we have truncated the above spectral series and for this purpose have employed the triangular scheme of Klaassen & Peltier (1985*b*), namely $2 \mid \lambda \mid +\nu \leqslant N_t$, where N_t is a global truncation level.

Equation (2.12) may also be rewritten in an equivalent vector form by concatenating the Galerkin amplitudes so as to form a vector $\boldsymbol{v}$. This leads to the equation

$$\frac{\mathrm{d}\boldsymbol{v}}{\mathrm{d}t} = \boldsymbol{A}(t)\boldsymbol{v}, \quad \boldsymbol{v} = \begin{pmatrix} u_{\lambda\nu} \\ w_{\lambda\nu} \end{pmatrix}, \tag{2.14}$$

in which the matrix $\boldsymbol{A}(t)$, which is in general time dependent, has elements which depend upon the four-dimensional spectral interaction coefficients (e.g. $\langle UU\rangle^{\kappa\mu}_{\lambda\nu}$, etc.). These spectral coefficients are listed in the Appendix for the inviscid problem of interest to us here. Depending upon the time dependence of the basic state two-dimensional flow, which determines the time dependence of the matrix $\boldsymbol{A}$, the solution of the evolution equation (2.14) could prove to be complicated indeed (e.g. Baym

1968; Drazin & Reid 1981). In the present context, however, our focus will be upon the stability characteristics of the steady two-dimensional Stuart model of vortical basic states in which case $\boldsymbol{A}$ is time independent. In such circumstances we may safely assume that temporal growth of the solution is exponential as $\boldsymbol{v} = \boldsymbol{v}_n e^{\sigma_n t}$, and (2.14) then reduces to the standard matrix eigenvalue problem:

$$\sigma_n \boldsymbol{v}_n = \boldsymbol{A}\boldsymbol{v}_n \tag{2.15}$$

in which σ_n, the eigenvalue of $\boldsymbol{A}$, is an exponential (in general complex) growth rate, $\boldsymbol{v}_n$ is the eigenvector corresponding to this eigenvalue and $\boldsymbol{A}$ is a time-independent stability matrix (with elements listed in the Appendix) corresponding to some two-dimensional vorticity distribution.

3. Columnar vortex stability: the Stuart model

In this section we will discuss the stability of Stuart vortices to three-dimensional perturbations as a function of the ellipticity parameter ρ. Because the length of the computational domain of the two-dimensional flow equals the wavelength of the train of coherent structures, the secondary instability analyses deliver only unstable modes whose streamwise wavelength equals that of the primary wave. The global truncation level for our analyses is set to $N_t = 37$ (significantly higher than it was possible to achieve in the work of Smyth & Peltier 1994) for all analyses of unstratified flows and it was shown through detailed comparative analyses (not shown) that all of the results to be reported herein are not significantly altered by further increase of this parameter. We will not explore the influence of stratification herein in order to focus upon comparison with the results of Leblanc & Cambon (1998). Through explicit analysis it has been shown in the previous work of Potylitsin & Peltier (1998) that sufficiently strong density stratification stabilizes two-dimensional columnar structures to disruption by modes of three-dimensional instability that exist even in the absence of rotation. In many cases the rate of stabilization depends on the nature of the instability. On the other hand, the viscosity of the fluid obviously introduces a short-wave cutoff in the growth rate as the spanwise wavenumber rises. The same behaviour is also characteristic of the spectrum of the Stuart model and it is therefore unnecessary to provide further discussion of the viscous case herein.

3.1. *The case of high ellipticity*

We begin presentation of the results of the stability analysis with those for the highly elliptical case of the Stuart vortices with the vortex parameter $\rho = 0.33$ (see figure 2*a*). Results for this case have been discussed recently by Leblanc & Cambon (1998) using a method of analysis that differs significantly from our own. We will provide a thorough reanalysis of this case in order to fix ideas and to enable us to connect the new results that we will obtain to this previous literature. As previously discussed, we will assume the rotation to be characterized by a constant angular frequency $\Omega = \frac{1}{2}f$, where f is the so-called Coriolis parameter which appears in the context of analyses of geophysical flows where it represents the local vertical component of the angular velocity of the planet. The vector of background rotation is parallel to the y-axis, so that the background vorticity, represented by $\boldsymbol{f}$, is either aligned with or against the relative vorticity field $\boldsymbol{\omega}$ of the two-dimensional flow (see figure 1). Note also that, in the case illustrated, the relative vorticity of the two-dimensional flow is positive while the vector $\boldsymbol{f}$ points in the negative direction along the y-axis. In this case the vorticity distribution is characterized as being anticyclonic.

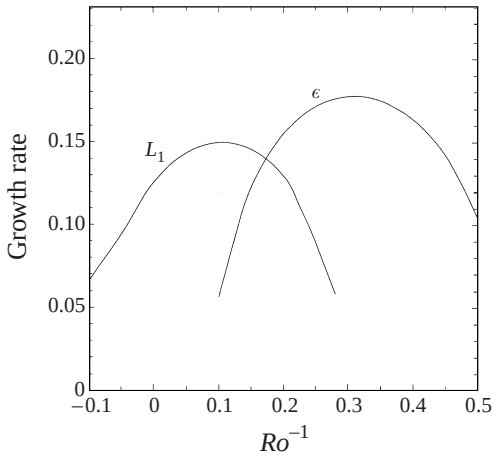

FIGURE 3. The instability spectrum for rotating unstratified Stuart vortices with the vortex parameter $\rho = 0.33$, with $d = 2$ and $Fr^{-2} = 0$, as a function of inverse Rossby number $Ro^{-1} = f/(U/L)$. The plot shows only the most unstable modes. The spatial structures of these modes are displayed in figures 4 and 5.

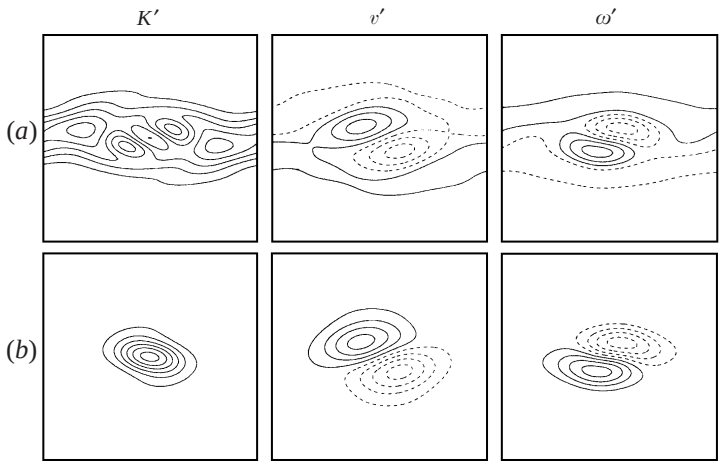

FIGURE 4. The perturbation kinetic energy K', spanwise velocity v' and spanwise vorticity ω' fields in the (X, Z)-plane for (*a*) the L_1 longitudinal mode at the point $d = 2.0$, $Ro^{-1} = 0.1$ and (*b*) the ϵ elliptical mode at the point $d = 2.0$, $Ro^{-1} = 0.3$. The vortex parameter $\rho = 0.33$. Solid lines show isolines with positive values while dashed lines represent isolines with negative values. The visual non-dimensional size of the domain is $2\pi \times 2\pi$.

In figure 3, we plot the growth rates, σ, of the most unstable modes for the Stuart vortex with the vortex parameter $\rho = 0.33$ as a function the inverse Rossby number $Ro^{-1} = f/(U/L)$, positive values of which therefore implying that the vorticity in the columnar vortices is anticyclonic. The non-dimensional spanwise wavenumber for these calculations was set to $d = 2.0$. This spectrum is determined by the eigenvalues of the stability matrix, and in it all modes are stationary (i.e. their growth rates are purely real). The entire set of modes with growth rates higher than $\sigma = 0.12$ at any Rossby number is displayed on this figure.

The modal branch labelled L_1 with the maximum growth rate in the vicinity of

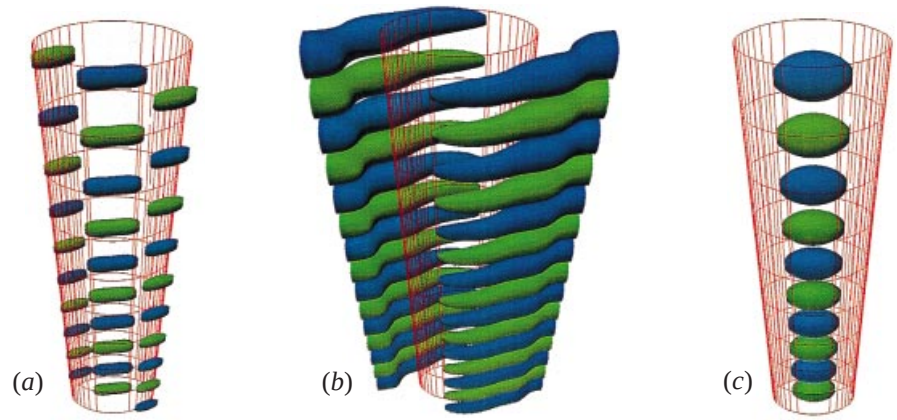

FIGURE 5. The entire family of instabilities for the Stuart model with $\rho = 0.33$. Isosurfaces of x-component of the perturbation vorticity field for (a) the core-centred longitudinal L_1 mode at $d = 2.0$, $Ro^{-1} = 0.0$, (b) the braid-centred longitudinal L_1 mode at $d = 3.0$, $Ro^{-1} = 0.0$ and (c) the z-component for the elliptical mode labelled ϵ in the text at $d = 2.0$, $Ro^{-1} = 0.3$.

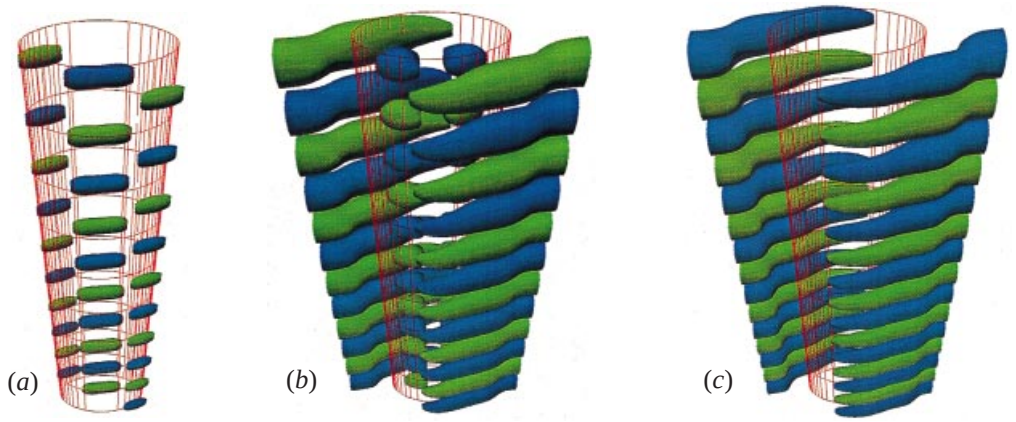

FIGURE 8. The smooth transition between the core-centred elliptical and braid-centred hyperbolic modes for the L_1 longitudinal branch of instability with $\rho = 0.33$. Isosurfaces of the x-component of the perturbation vorticity field for (a) the core-centred longitudinal L_1 mode at $d = 2.0$, $Ro^{-1} = 0.0$ (b) the transition state of the L_1 mode at $d = 2.4$, $Ro^{-1} = 0.0$ and (c) the braid-centred longitudinal L_1 mode at $d = 3.0$, $Ro^{-1} = 0.0$.

zero background rotation represents a branch of longitudinal modes (Smyth & Peltier 1994) and is the counterpart in the present analysis of the structure first identified by Klaassen & Peltier (1991). Note that in the present case the mode exhibits maximum growth rate at the point $Ro^{-1} = 0.1$, while in the case of the Kelvin–Helmholtz background flow (Smyth & Peltier 1994) the L_1 mode has maximum growth rate for precisely zero background rotation. The spatial structure of the mode at the point $Ro^{-1} = 0.1$ is displayed in figure 4(a) in terms of its spatial distribution of perturbation kinetic energy K', spanwise velocity v' and spanwise vorticity ω' in the (X, Z)-plane. The perturbation kinetic energy is quadratic in the disturbance fields, and the figure displays the average of this quantity over a single spanwise wavelength in the form of a positive real function of x and z. The spanwise velocity

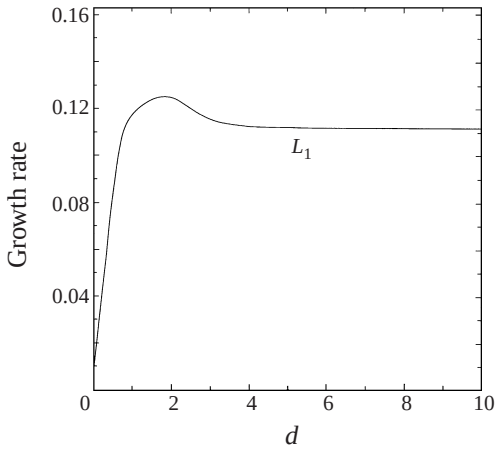

FIGURE 6. The instability spectrum for non-rotating Stuart vortices with the vortex parameter $\rho = 0.33$, with $Ro^{-1} = 0$ and $Fr^{-2} = 0$, as a function of wavenumber d. The plot shows only the most unstable mode. The spatial structures of these modes are displayed in figure 7.

and vorticity perturbations vary sinusoidally with y, and the corresponding parts of the figure for these eigenfunctions show the corresponding fields evaluated on a plane of constant y, which has been chosen to coincide approximately with the maximum of the perturbation quantity. The modal structure displayed in figure 4(a) is somewhat core-centred, i.e. the perturbation fields achieve an extremum in the vicinity of the core of the two-dimensional elliptical billows but they also have significant power on the hyperbolic stagnation points.

The other branch of modes shown on figure 3 (labelled ϵ) represents a highly core-centred mode with purely real growth rate. This mode achieves its maximum growth near the point $Ro^{-1} = 0.3$ and its growth rate exceeds the maximum growth rate of the L_1 longitudinal mode. The spatial structure of the mode is shown in figure 4(b). It is indeed tightly confined to the core and we could find no counterpart of this mode in the non-rotating problem (Potylitsin & Peltier 1998). This branch is therefore identified as comprising elliptical modes modified by the Coriolis force because it exists only for elliptical vortices (see discussion of the results for the circular limit of the 'Kida-like' vortex in Potylitsin & Peltier 1998). In figures 5(a) and 5(b) we illustrate the L_1 longitudinal mode of instability for the Stuart model with the vortex parameter $\rho = 0.33$, the inverse Rossby number $Ro^{-1} = 0$ and for the two respective values of the cross-stream wavenumber $d = 2.0$ and $d = 3.0$, in the form of isosurface renderings of the perturbation vorticity field. In figure 5(c) the structure of the elliptical ϵ mode at $Ro^{-1} = 0.3$ and $d = 2.0$ is also illustrated.

As the spanwise wavenumber d rises the growth rate of the unstable modes on the L_1 branch at first increases monotonically (Smyth & Peltier 1994) eventually reaching a limiting value which depends on the Rossby number. In figure 6, we plot the growth rate, σ, of the most unstable mode of the Stuart vortex as a function of the spanwise wavenumber d at the point $Ro^{-1} = 0$. Inspection of the spatial structure of the modes along this branch reveals that it changes abruptly from core-centred at low d to braid-centred form at high d. The spatial structure of the mode at the point $d = 2.0$ is displayed in figure 7(a) in terms of its spatial distribution of perturbation kinetic energy K', spanwise velocity v' and spanwise vorticity ω' in the (X, Z)-plane. The

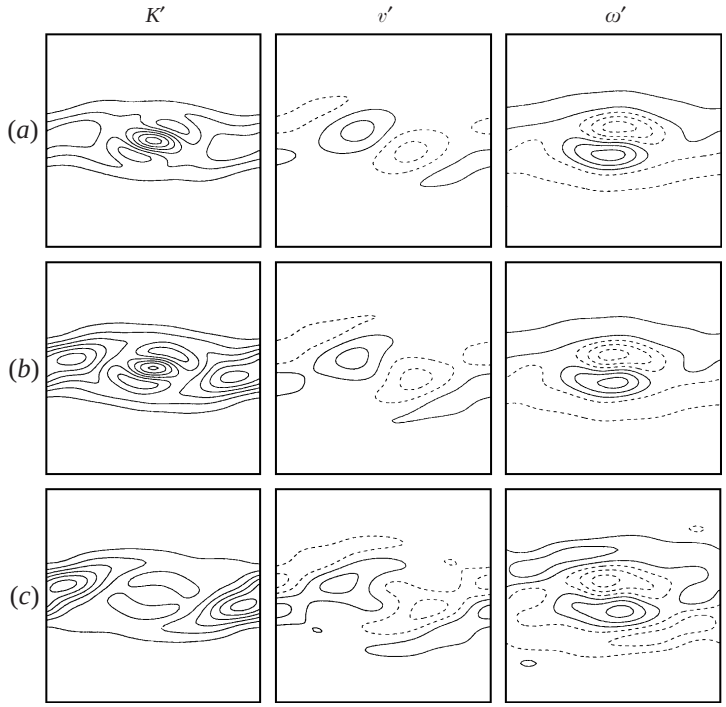

FIGURE 7. The perturbation kinetic energy K', spanwise velocity v' and spanwise vorticity ω' fields in the (X, Z)-plane for the L_1 longitudinal mode, (a) at the point $d = 2.0$, (b) $d = 2.4$ and (c) $d = 3.0$. The vortex parameter $\rho = 0.33$ and the inverse Rossby number $Ro^{-1} = 0.0$. Solid lines show isolines with positive values while dashed lines represent isolines with negative values. The visual non-dimensional size of the domain is $2\pi \times 2\pi$.

modal structure displayed in figure 7(a) is core-centred, i.e. the perturbation fields are focused in the vicinity of the core of the two-dimensional elliptical billows.

Considering next the spatial structure of the same L_1 mode but at the point $d = 3.0$ (see figure 7c), we note that the kinetic energy perturbation is now centred on the hyperbolic stagnation points located between individual vortex cores. Since our interest in this paper is primarily in the stability of isolated columnar vortices it should be clear that only the core-centred modes of the L_1 branch would exist on an isolated vortex tube since in that circumstance the hyperbolic regions do not exist. It is also interesting to note that a smooth transition between core-centred and braid-centred modal structure exists. The characteristic spatial structure of the L_1 mode in this transition region is shown in figure 7(b). Core-centred and braid-centred perturbations of the same intensity coexist. In figure 8 (page 216) we illustrate the smooth transition between the core-centred elliptical mode and the braid-centred hyperbolic mode in the form of isosurface renderings of the streamwise (x) component of the perturbation vorticity field. While at high spanwise wavenumber ($d > 3.0$) the modal structure of the L_1 longitudinal mode changes abruptly from core-centred at low d to braid-centred (Smyth & Peltier 1994), the modal structure of the ϵ elliptical mode does not exhibit the same sensitivity to the change in cross-stream scale.

It is quite clear on the basis of these results that the L_1 longitudinal core-centred mode corresponds to the so-called 'translative' or elliptical instability (Pierrehumbert & Widnall 1982; Bayly 1986; Waleffe 1990; Klaassen & Peltier 1985, 1989, 1991) in that the perturbation vorticity field ω' describes a translation of each vortex in

the train of Stuart vortices in the same direction, a direction that varies sinusoidally along the axis of the basic-state vortex tube. Under the assumption that nonlinearity does not alter the fundamental character of the instability, we may infer the way in which the originally columnar vortex would be altered by the growth of the linearly unstable mode. Because the vorticity perturbation is sinusoidal in the y-direction, the translative instability would initially induce bending of the vortex tubes in a sinusoidal fashion with the wavelength corresponding to the most unstable wavelength in the spectrum (Pierrehumbert & Widnall 1982). However, there exists another fast growing instability in the L_1 branch of the spectrum, which is not core-centred but rather is centred on the hyperbolic stagnation point. The latter, which derives from what we might refer to as 'hyperbolic' instability, is the origin of the streamwise vortex streaks whose appearance is precursory to the turbulent collapse of the unstratified mixing layer (Klaassen & Peltier 1985*b*, 1991; Smyth & Peltier 1991, 1994; Caulfield & Peltier 1994). It is also worth repeating that in the spectrum of the Stuart model an intermediate regime is also observed in which elliptical and hyperbolic instability coexist (see figure 7*b*).

It will be noted that our result is identical to the result obtained recently by Leblanc & Cambon (1998) for the Stuart vortex with the vortex parameter $\rho = 0.33$, although these authors were unable to distinguish the core-centred branch of the L_1 longitudinal modes nor were they able to identify the hyperbolic branch of the L_1 instability.

3.2. *The case of moderate ellipticity*

Having both confirmed and extended the previous results obtained by Leblanc & Cambon (1998) for the instability of the Stuart model with the ellipticity parameter $\rho = 0.33$, we are in a good position to extend this work to consider Stuart vortices with lower ellipticity. In this next step of the analysis, we wish to examine the influence of the ellipticity of a vortex on the dominant modes of three-dimensional instability of the vortex column under the action of background rotation. We will therefore focus next upon the stability characteristics of the Stuart model with the vortex parameter $\rho = 0.50$ (see figure 2*b*). The stability analyses for this and higher values of the vortex parameter ρ are more complicated and require more careful analysis and higher spatial resolution because of the nature of the stagnation point at the centre of the Stuart vortex core. Our choice of the truncation level $N_t = 37$ was determined on the basis of this being the level required to achieve convergence of the results for these structures.

Figure 9 presents growth rates of the most unstable modes as a function of inverse Rossby number (Ro^{-1}) with the spanwise wavenumber $d = 2.0$ for Stuart vortices with the vortex parameter $\rho = 0.50$. If one compares this instability spectrum with that for the Stuart vortices with the vortex parameter $\rho = 0.33$ (see figure 3), it is very clear that a high degree of similarity exists. The dominant mode (labelled ϵ) in the spectrum for the anticyclonic vortex, when the background rotation is relatively slow, once more has purely real growth rate. The eigenfunctions that determine the spatial localization of this mode are again concentrated in the core of the background vortex and the spatial structure of the mode (not shown here) is therefore similar to the ϵ elliptical mode when the vortex parameter $\rho = 0.33$ (see figure 4*b*). The most unstable point for this mode is slightly shifted to lower values of background rotation compared to that in the instability spectrum in figure 3.

The branch of modes with maximum growth rate for small Ro^{-1} may be identified as the L_1 longitudinal mode and clearly corresponds to the L_1 mode for the Kelvin–

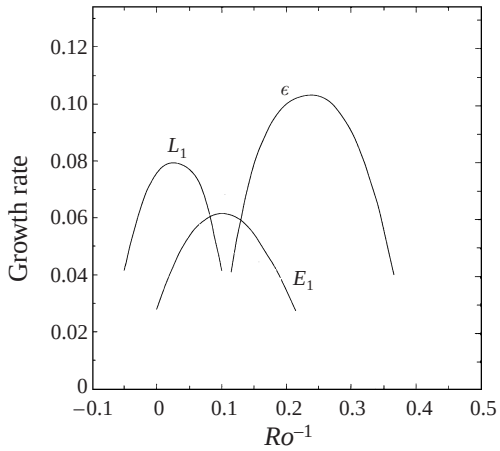

FIGURE 9. The instability spectrum for rotating unstratified Stuart vortices with the vortex parameter $\rho = 0.50$, with $d = 2$ and $Fr^{-2} = 0$, as a function of inverse Rossby number $Ro^{-1} = f/(U/L)$. The plot shows only the most unstable modes. The spatial structures of these modes are displayed in figure 10.

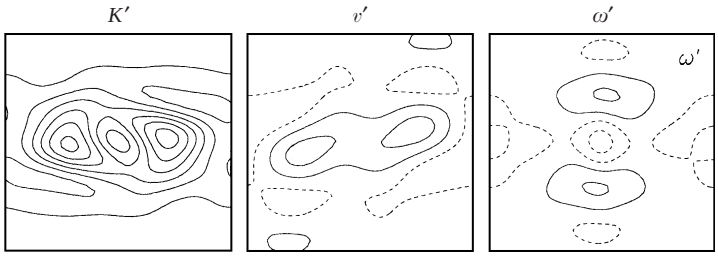

FIGURE 10. The perturbation kinetic energy K', spanwise velocity v' and spanwise vorticity ω' fields in the (X, Z)-plane for the edge E_1 mode at the point $d = 2.0$, $Ro^{-1} = 0.1$. The vortex parameter $\rho = 0.50$. Solid lines show isolines with positive values while dashed lines represent isolines with negative values. The visual non-dimensional size of the domain is $2\pi \times 2\pi$.

Helmholtz vortex (Smyth & Peltier 1994). The point of maximum growth rate along the L_1 branch of modes corresponds to precisely zero background rotation. The modal structure of this mode for $d = 2.0$ is braid-centred, although it once more changes to a core-centred form at lower spanwise wavenumbers.

The final branch of modes shown in figure 9 (labelled E_1) represents a new type of instability which was not observed for Stuart vortices with lower values of the vortex parameter ρ. Its perturbation kinetic energy (see figure 10) is seen to be concentrated

FIGURE 11. The entire family of instability for the Stuart model with $\rho = 0.50$. Isosurfaces for the x-component of the perturbation vorticity field for (a) the core-centred longitudinal L_1 mode at $d = 0.5$, $Ro^{-1} = 0.0$, (b) the braid-centred longitudinal L_1 mode at $d = 2.0$, $Ro^{-1} = 0.0$; and the z-component for (c) the edge E_1 mode at $d = 2.0$, $Ro^{-1} = 0.1$, (d) the elliptical mode ϵ at $d = 2.0$, $Ro^{-1} = 0.25$.

FIGURE 14. The entire family of instability for the Stuart model with $\rho = 0.75$. Isosurfaces of the x-component of the perturbation vorticity field for (a) the core-centred longitudinal L_1 mode at $d = 0.5$, $Ro^{-1} = 0.0$ and (b) the braid-centred longitudinal L_1 mode at $d = 2.0$, $Ro^{-1} = 0.0$; (c) the z-component for the edge E_0 mode at $d = 2.0$, $Ro^{-1} = 0.3$ and (d) the x-component for the elliptical mode ϵ at $d = 2.0$, $Ro^{-1} = 0.2$.

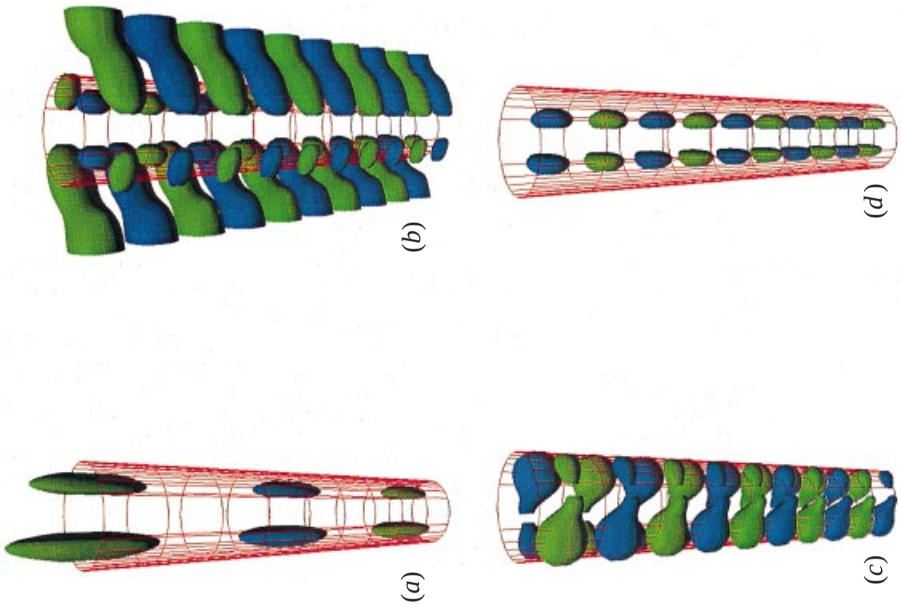

FIGURE 14

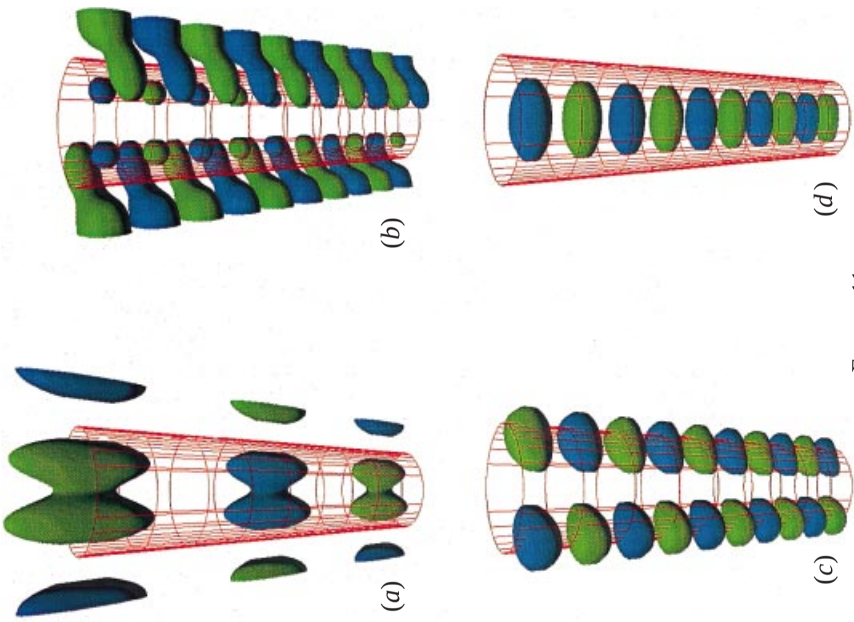

FIGURE 11

FIGURE 11 and FIGURE 14. For captions see facing page.

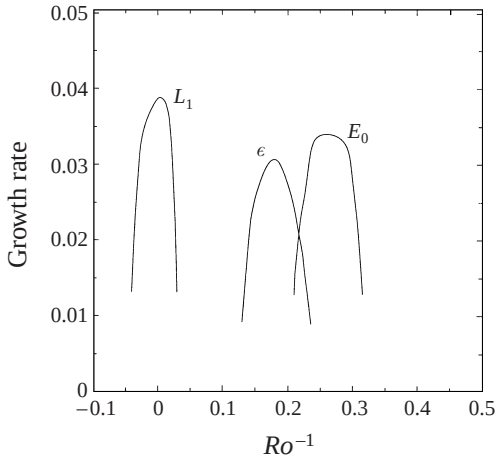

FIGURE 12. The instability spectrum for rotating unstratified Stuart vortices with the vortex parameter $\rho = 0.75$, with $d = 2$ and $Fr^{-2} = 0$, as a function of inverse Rossby number $Ro^{-1} = f/(U/L)$. The plot shows only the most unstable modes. The spatial structures of these modes are displayed in figure 13.

in a ring surrounding the core of the background vortex, so that, following Smyth & Peltier (1994), this mode will be referred as the edge mode. The E_1 mode achieves its maximum growth rate at $Ro^{-1} = 0.1$. The E_1 branch can also be identified as the first harmonic of an edge mode sequence as we will see. In figure 11 we illustrate all modes of instability for the Stuart model with the vortex parameter $\rho = 0.50$ in the form of isosurface renderings of the perturbation vorticity field.

The E_1 mode represents an entirely new class of modes which has no counterpart in the non-rotating problem. It was pointed out in Smyth & Peltier (1994) that the physical mechanism of instability for the edge mode is most usefully understood in terms of the inertial (centrifugal) mechanism. In the case of the Kelvin–Helmholtz vortex, the spatial location (Potylitsin & Peltier 1998) of the edge mode corresponds quite closely to the region in which the modified Rayleigh criterion (e.g. Kloosterziel & van Heijst 1991) is violated for an anticyclonic vortex when the background rotation is relatively slow and, therefore, suggests the possibility of instability.

3.3. *The limit of low ellipticity*

The further issue that clearly arises from these analyses concerns the dominant mechanism of instability for the vortices with small ellipticity which are most frequently observed in geophysical flows. It might be expected that the centrifugal mechanism could dominate in this case. To investigate the validity of this expectation we have also performed a similar instability analysis for the almost circular case of the Stuart vortex with the vortex parameter $\rho = 0.75$.

The instability spectrum for this case with spanwise wavenumber $d = 2.0$ is shown in figure 12. Only the most unstable modes are presented. As expected, the general form of the spectrum is similar to results obtained in the previous analyses. The L_1 longitudinal mode is again dominant in the vicinity of zero background rotation but this mode is rapidly extinguished as the rate of rotation increases. The eigenvectors of this mode for the wavenumber $d = 2.0$ are similar to the braid-centred structure presented in figure 4(*b*) and therefore are not shown here. The most unstable mode for the inverse Rossby number $Ro^{-1} = 0.2$ can be identified as the elliptical (ϵ) mode. This

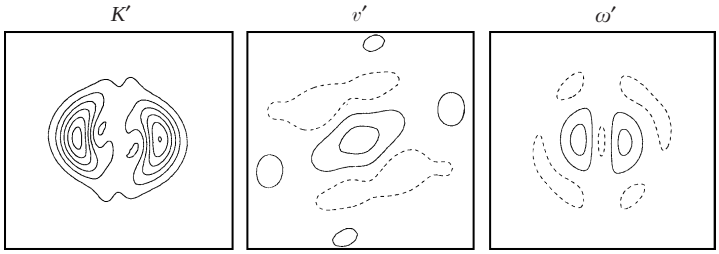

FIGURE 13. The perturbation kinetic energy K', spanwise velocity v' and spanwise vorticity ω' fields in the (X, Z)-plane for the edge E_0 mode at the point $d = 2.0$, $Ro^{-1} = 0.25$. The vortex parameter $\rho = 0.75$. Solid lines show isolines with positive values while dashed lines represent isolines with negative values. The visual non-dimensional size of the domain is $2\pi \times 2\pi$.

mode is an elliptical instability modified by the Coriolis force. The main difference in the spectrum for this almost circular case from those with higher ellipticity is that the E_0 fundamental harmonic of the edge mode family now appears in the spectrum. This mode represents the dominant instability for strong anticyclonic vortices with this ellipticity. The maximum growth rate for the edge mode now exceeds the maximum growth rate for the elliptical (ϵ) mode, which was the dominant mode of instability for Stuart vortices with higher ellipticity. The spatial structure of the mode is illustrated in figure 13. Similarly to the first harmonic of the edge mode family, the perturbation kinetic energy is concentrated in a ring around the two-dimensional core of the vortex. In figure 14 (page 221) we illustrate all modes of instability for the Stuart model with the vortex parameter $\rho = 0.75$ in the form of isosurface renderings of the perturbation vorticity field.

On the basis of this example, we may conclude that the general behavior of the unstable modes and thus the instability mechanisms for the rotating case of the Stuart model vortex with low ellipticity are very similar to those for the Kelvin–Helmholtz and 'Kida-like' vortices investigated in the previous work of Smyth & Peltier (1994) and Potylitsin & Peltier (1998) respectively, where the edge mode family was shown to be the dominant instability mechanism for strong anticyclones. Note that the elliptical ϵ mode has also been shown to be present in the spectrum of the Kelvin–Helmholtz and 'Kida-like' vortices with sufficiently high ellipticity (Potylitsin & Peltier 1998).

4. Summary

The goal of the analyses presented herein has been to investigate the dependence of the linear stability of two-dimensional columnar vortex basic states in a rotating environment to three-dimensional perturbations. We have focused upon the ellipticity of the vortex columns and the nature of the instabilities to which they are subject. We thereby sought to demonstrate the link between results obtained in recent work by Leblanc & Cambon (1998) in which the elliptical instability modified by background rotation was found to be dominant for strong anticyclones and the earlier work by Smyth & Peltier (1994) and Potylitsin & Peltier (1998) in which the centrifugal instability was found to be the dominant mode for the same rate of background rotation. Our goal in this paper has been to provide a detailed assessment of the circumstances in which these unstable modes may appear.

The model selected for the background vorticity distribution in the columnar vortices was taken herein to be that provided by the Stuart model for various choices of the vortex parameter. For the purpose of these analyses, it was assumed that the

basic-state rotation may be either positive (in the same sense as the vorticity in the column), which corresponds to the cyclonic vortex in our context, or negative (in the opposite sense), which corresponds to the anticyclonic vortex. The influence of rotation on the stability characteristics of the flows has been included in the f-plane approximation.

The methodology that we have developed for performing such theoretical linear stability analyses is by now well-known. It enables us to reduce the three-dimensional linear perturbation equations that determine the stability of a two-dimensional basic state into the form of a standard matrix eigenvalue problem whose solution reveals the instability characteristics of the two-dimensional background flow.

In the first step of our analysis, we both recovered and extended the results of previous analyses by Leblanc & Cambon (1998) for the Stuart vortex train in a rotating environment. We focused on the stability of a train of two-dimensional highly elliptical Stuart vortices with the vortex parameter $\rho = 0.33$. It was found that the spectrum of three-dimensional instability is dominated at low background rotation $Ro^{-1} \approx 0$ by the L_1 longitudinal mode. At low spanwise wavenumber the instability for this branch is characterized by the core-centred segment of elliptical instability in which the perturbation kinetic energy is concentrated in the vortex cores, but for high wavenumbers by the segment of hyperbolic instability in which the perturbation kinetic energy is concentrated in the strained regions between the primary vortices. These analyses also confirm the results reported previously by Smyth & Peltier (1994), which were conducted for Kelvin–Helmholtz billows at lower resolution. For strong anticyclonic vortices the maximum destabilization was found to occur in the vicinity of the point $Ro^{-1} = 0.3$. The perturbation kinetic energy of the mode labelled ϵ was shown to be concentrated in the core of the two-dimensional vortex. The mechanism for this mode has been identified as an elliptical instability modified by background rotation. This mode was first identified by Potylitsin & Peltier (1998) in their stability analyses of elliptical Kelvin–Helmholtz billows in the presence of rotation, although it was found to be dominant only in a very narrow interval in the vicinity of the point $Ro^{-1} = 0.3$. It will also be noted that our result is identical to that recently obtained by Leblanc & Cambon (1998) for Stuart vortices with vortex parameter $\rho = 0.33$, although these authors failed to distinguish the core-centred branch of the L_1 longitudinal mode as well as to identify the braid-centred hyperbolic branch of the L_1 instability.

In the next step, we performed three-dimensional analyses of the Stuart vortex with lower ellipticity, namely for the vortex parameter $\rho = 0.50$. Maximum destabilization for this case was found in the vicinity of the point $Ro^{-1} = 0.25$. This instability was identified as the same ϵ elliptical mode as was revealed in the previous case of the highly elliptical vortex. A further type of instability, however, was found to be dominant in a narrow region near the point $Ro^{-1} = 0.1$. The perturbation kinetic energy of this mode was shown to be concentrated in a ring surrounding the core of the two-dimensional vortex and, therefore, we continue to refer to this mode, following Smyth & Peltier (1994), as the edge mode. On the basis of the previous work by Smyth & Peltier (1994) and Potylitsin & Peltier (1998) we gave good reason to believe that the mechanism that underlies the edge mode is essentially centrifugal. The spatial location of the edge modes does indeed correspond in an approximate sense to the region in which the modified Rayleigh stability criterion is violated. No analysis of the rotating Stuart vortex has previously revealed the existence of the centrifugal mode.

The final aspect of the coherent structure destruction mechanisms analysed herein

involved an investigation of the Stuart vortex with low ellipticity ($\rho = 0.75$). Through analyses of this case we demonstrated that the edge mode becomes the dominant mechanism of instability for vortices with low ellipticity, although the elliptical ϵ mode still remains in the instability spectrum. The maximum growth rate for the E_0 edge mode exceeds the growth rate for the elliptical ϵ mode for this value of ρ. This result is therefore very similar to the result obtained by Potylitsin & Peltier (1998) for Kelvin–Helmholtz and elliptical Kida-like vortices where the centrifugal instability mechanism was found to be dominant for strong anticyclones.

In further work it will be our intention to discuss the detailed nonlinear evolution of each of the linear secondary instabilities that our analyses have revealed, both in the present paper and in Smyth & Peltier (1994) and Potylitsin & Peltier (1998). It is only on the basis of such further investigation that we will be able to make closer contact with the experimental results of Kloosterziel & van Heijst (1991) and related investigations. A primary goal of this ongoing research is to understand which of the various modes of secondary instability is actually responsible for creating the finite-amplitude structures that experiments on columnar vortex stability have revealed.

Appendix

The coefficients of the four-dimensional submatrices in the matrix equation (2.12) are given by

$$(1+\delta_{\mu 0})\langle UU\rangle_{\lambda\nu}^{k\mu} = -\mathrm{i}\lambda\alpha\langle F_{k\mu}^{*}\tilde{U}F_{\lambda\nu}\rangle - \langle F_{k\mu}^{*}\tilde{U}_{x}F_{\lambda\nu}\rangle + D_{\nu}\langle F_{k\mu}^{*}\tilde{W}G_{\lambda\nu}\rangle + 2\frac{\lambda k\alpha^{2}}{A_{k\mu}}\langle F_{k\mu}^{*}\tilde{U}_{x}F_{\lambda\nu}\rangle + 2\frac{\mathrm{i}k\alpha D_{\nu}}{A_{k\mu}}\langle F_{k\mu}^{*}\tilde{W}_{x}G_{\lambda\nu}\rangle,$$

$$(1+\delta_{\mu 0})\langle UW\rangle_{\lambda\nu}^{k\mu} = -\langle F_{k\mu}^{*}\tilde{U}_{z}G_{\lambda\nu}\rangle + 2\frac{\lambda k\alpha^{2}}{A_{k\mu}}\langle F_{k\mu}^{*}\tilde{U}_{z}G_{\lambda\nu}\rangle - 2\frac{\mathrm{i}k\alpha D_{\nu}}{A_{k\mu}}\langle F_{k\mu}^{*}\tilde{W}_{z}F_{\lambda\nu}\rangle,$$

$$\langle WU\rangle_{\lambda\nu}^{k\mu} = -\langle G_{k\mu}^{*}\tilde{W}_{x}F_{\lambda\nu}\rangle + \frac{2\mathrm{i}\lambda\alpha D_{\mu}}{A_{k\mu}}\langle F_{k\mu}^{*}\tilde{U}_{x}F_{\lambda\nu}\rangle - \frac{2D_{\nu}D_{\mu}}{A_{k\mu}}\langle F_{k\mu}^{*}\tilde{W}_{x}G_{\lambda\nu}\rangle,$$

$$\langle WW\rangle_{\lambda\nu}^{k\mu} = -\mathrm{i}\lambda\alpha\langle G_{k\mu}^{*}\tilde{U}G_{\lambda\nu}\rangle - D_{\nu}\langle G_{k\mu}^{*}\tilde{W}F_{\lambda\nu}\rangle - \langle G_{k\mu}^{*}\tilde{W}_{z}G_{\lambda\nu}\rangle + 2\frac{\mathrm{i}\lambda\alpha D_{\mu}}{A_{k\mu}}\langle F_{k\mu}^{*}\tilde{U}_{z}F_{\lambda\nu}\rangle + \frac{2D_{\mu}D_{\nu}}{A_{k\mu}}\langle F_{k\mu}^{*}\tilde{W}_{z}F_{\lambda\nu}\rangle$$

in which $D_{\nu} = \nu\pi/H$ and $A_{\lambda\nu} = (\lambda\alpha)^{2} + d^{2} + D_{\nu}^{2}$.

REFERENCES

Bartello, P., Metais, O. & Lesieur, M. 1994 Coherent structures in rotating three-dimensional turbulence. *J. Fluid Mech.* **273**, 1–29.

Bayly, B. J. 1986 Three-dimensional instability of elliptical flow. *Phys. Rev. Lett.* **57**, 2160–2163.

Baym, G. 1968 *Lectures on Quantum Mechanics*. W. A. Benjamin.

Bernal, L. P. & Roshko, A. 1986 Streamwise vortex structure in plane mixing layeres. *J. Fluid Mech.* **170**, 499–525.

Browand, F. K. & Ho, C. M. 1983 The mixing layer: an example of quasi two-dimensional turbulence. *J. Mec. Theor. Appl.* 99–120.

Cambon, C., Benoit, J.-P., Shao, L. & Jacquin, L. 1994 Stability analysis of large eddy simulation of rotating turbulence with organized eddies. *J. Fluid Mech.* **278**, 175–200.

Carnevale, G. F., Briscolini, M., Kloosterziel, R. C. & Vallis, G. K. 1997 Three-dimensionally perturbed vortex tubes in a rotating flow. *J. Fluid Mech.* **341**, 127–163.

Caulfield, C. P. & Peltier, W. R. 1994 Three dimensionalization of the stratified mixing layer. *Phys. Fluids* **6**, 3803–3805.

Corcos, G. M. & Lin, S. J. 1984 The mixing layer: deterministic models of a turbulent flow. Part 2. The origin of the three-dimensional motion. *J. Fluid Mech.* **139**, 67–95.

Corcos, G. M. & Sherman, F. S. 1984 The mixing layer: deterministic models of a turbulent flow. Part 1. Introduction and the two-dimensional flow. *J. Fluid Mech.* **139**, 29–65.

Drazin, P. G. & Reid, W. H. 1981 *Hydrodynamic Stability*. Cambridge University Press.

Etling, D. 1990 Mesoscale vortex shedding from large islands: a comparison with laboratory experiments of rotating stratified flows. *Metl. Atmos. Phys.* **43**, 145–151.

Hopfinger, E. J., Browand, F. K. & Gagne, Y. 1982 Turbulence and waves in a rotating tank. *J. Fluid Mech.* **125**, 505–534.

Kida, S. 1981 Motion of an elliptic vortex in a uniform shear flow. *J. Phys. Soc. Japan* **50**, 3517–3520.

Klaassen, G. P. & Peltier, W. R. 1985*a* Evolution of finite amplitude Kelvin–Helmholtz billows in two spatial dimensions. *J. Atmos. Sci.* **42**, 1321–1339.

Klaassen, G. P. & Peltier, W. R. 1985*b* The onset of turbulence in finite-amplitude Kelvin–Helmholtz billows. *J. Fluid Mech.* **155**, 1–35.

Klaassen, G. P. & Peltier, W. R. 1989 The role of transverse secondary instabilities in the evolution of the shear layers. *J. Fluid Mech.* **202**, 367–402.

Klaassen, G. P. & Peltier, W. R. 1991 The influence of stratification on secondary instability in free shear layers. *J. Fluid Mech.* **227**, 71–106.

Kloosterziel, R. C. & Heijst, G. J. F. van 1991 An experimental study of unstable barotropic vortices in a rotating fluid. *J. Fluid Mech.* **223**, 1–24.

Lasheras, J. C., Cho, J. S. & Maxworthy, T. 1986 On the origin and evolution of streamwise vortical structures in a plane, free shear layer. *J. Fluid Mech.* **172**, 231–258.

Lasheras, J. C. & Choi, H. 1988 Three-dimensional instability of a plane free shear layer: an experimental study of the formation and evolution of streamwise vortices. *J. Fluid Mech.* **189**, 53–86.

Leblanc, S. & Cambon, C. 1998 Effects of the Coriolis force on the stability of Stuart's vortices. *J. Fluid Mech.* **356**, 353–379.

Nygaard, K. J. & Glezer, A. 1991 Evolution of streamwise vortices and generation of small-scale motions in a plane mixing layer. *J. Fluid Mech.* **231**, 257–301.

Pierrehumbert, R. T. 1986 Universal short-wave instability of two-dimensional eddies in an inviscid fluid. *Phys. Rev. Lett.* **57**, 2157.

Pierrehumbert, R. T. & Widnall, S. E. 1982 The two- and three-dimensional instabilities of a spatially periodic shear layer. *J. Fluid Mech.* **114**, 59–82.

Potylitsin, P. G. & Peltier, W. R. 1998 Stratification effects on the stability of columnar vortices on the f-plane. *J. Fluid Mech.* **355**, 45–79.

Schowalter, D. G., Van Atta, C. W. & Lasheras, J. C. 1994 A study of streamwise vortex structures in a stratified shear layer. *J. Fluid Mech.* **281**, 247–291.

Smyth, W. D. & Peltier, W. R. 1989 The transition between Kelvin–Helmholtz and Holmboe instability: an investigation of the overreflection hypothesis. *J. Atmos Sci.* **46**, 3698–3720.

Smyth, W. D. & Peltier, W. R. 1991 Instability and transition in finite-amplitude Kelvin–Helmholtz and Holmboe waves. *J. Fluid Mech.* **228**, 387–415.

Smyth, W. D. & Peltier, W. R. 1994 Three-dimensionalization of barotropic vortices on the f-plane. *J. Fluid Mech.* **265**, 25–64.

Stuart, J. T. 1967 On finite amplitude oscillations in laminar mixing layers. *J. Fluid Mech.* **29**, 417–440.

Waleffe, F. 1990 On the three-dimensional instability of strained vortices. *Phys. Fluids* A **2**, 76–80.

Winant, C. D. & Browand, F. K. 1974 Vortex pairing: the mechanism of turbulent mixing layer growth at moderate Reynolds numbers. *J. Fluid Mech.* **63**, 237–255.

Wygnanski, I., Oster, D., Fiedler, H. & Dziomba, B. 1979 On the perseverance of quasi-two-dimensional eddy structures in a turbulent mixing layer. *J. Fluid Mech.* **93**, 325–335.